Monografías de la Real Academia de Ciencias de Zaragoza **34**, 51–71, (2010).

Forest Fire Simulation: Mathematical Models and Numerical Methods

L. Ferragut[†], M.I. Asensio[†] and J. Simon[‡]

[†] IUFFyM Instituto Universitario de Física Fundamental y Matemáticas.
Universidad de Salamanca, plaza. Merced s/n, 37008 Salamanca, Spain

[‡]CNRS & Laboratoire Jean Alexandre Dieudonné.
Université de Nice, Parc Valrose, 06108 Nice, cedex 2, France

Abstract

At present, there exists a wide range of fire behavior models and studies aiming to simulate fire. After a brief review of fire spread models we focus on physical models. Physical or combustion models describe the evolution of physical quantities inside the vegetation, considered as a porous medium, and as a consequence provide the evolution of the fire front. Between combustion models we can distinguish two groups:

1. Complex models, where general conservation laws are considered and several phases, solid phase and gas phase with different temperatures, two layers models, etc.
2. Simplified models, where in general an average media is considered with average magnitudes. Usually only one temperature is considered and only one phase (the other phase is parameterized). The simplified models are more realistic than models based on cellular automata, geometric models and other empirical models, but allow faster computations than complex models, providing computation times below real time and at the same time taking into account the main physical mechanisms concerning the fire propagation.

This models takes into account three of the main mechanisms in fire spread, namely, Water content, Radiation qnd Wind and topography effects. We will discuss also some aspects concerning the numerical methods involved.

Keywords: Forest fires, moisture, radiation, wind

1 Introduction

Fire modelling is a highly challenging problem from both the physical and the numerical point of view, which forces. From the more simple and empirical models to the more complex theoretical models, all of a compromise position among urge of practical usefulness, computer capabilities and existing numerical methods.

The empirical models are based on empirical correlations found on actual fires and on documentation of the principle characteristics of different vegetation types. Among them we should mention the one develop by Rothermel [1], implemented in the well known software Behave, used in most of the North American forestry management offices. These models predict the position of the fire front, but many relevant physical variables of the fire are unknown. Since they rely in correlations obtained in real situations, their use with different physical conditions is hard.

Combustion models are based on balance laws of physics and intend to keep track of the real physical variables involved in a fire. They are usually posed on a bidimensional domain (for real time computations this is mandatory) representing the vegetation layer which is considered as a porous medium where the main variables of fire develop. Coupled to these equations through certain parameters, several important physical effects like wind, moisture, tilt or radiation are evaluated.

The general deduction and simplification of the initial three dimensional differential equations is complex as can be seen in [2] and [3]. Consequently equations are usually simply posed following plausible physical arguments. Despite of the relatively wide range of different approximations to the problem the basic structure of the differential equations to be solved usually conserve a common structure. The following adimensional equations may represent a simple but realistic model.

$$\frac{\partial e}{\partial t} + \mathbf{w} \cdot \nabla e - (J * u^4 - u^4) + \alpha u = A f(u, y) \tag{1}$$

$$e \in G(u) \tag{2}$$

$$\frac{\partial y}{\partial t} = -f(u, y) \tag{3}$$

Here e is the non-dimensional enthalpy, u is the non-dimensional temperature and y is the non-dimensional mass fraction of fuel.

The non-dimensional enthalpy e introduced accounts for moisture effects, and is an element of a multivalued maximal monotone operator G, given by:

$$G(u) = \begin{cases} u & \text{if} \quad u < u_v \\ [u_v \ , \ u_v + \lambda_v] & \text{if} \quad u = u_v \\ u + \lambda_v & \text{if} \quad u_v < u < u_p \\ [u_p + \lambda_v \ , \ u_p + \lambda_v + \lambda_p] & \text{if} \quad u = u_p \\ u + \lambda_v + \lambda_p & \text{if} \quad u > u_p \end{cases} \tag{4}$$

where u_v and u_p, are the non-dimensional evaporation temperature of the water and the non-dimensional pyrolysis temperature of the solid fuel, respectively. The quantities λ_v and λ_p are the non-dimensional evaporation heat and pyrolysis heat.

The right hand side functions f follow an Arrhenius type law and modelize on one side the loss of fuel and on the other the energy gain due to combustion. The term αu represents the energy lost by convection in the vertical direction.

If the medium is optically thick the non local radiation $-(J * u^4 - u^4)$ could be approximated by a non linear diffusion term plus an additional convection term if the kernel $J(\cdot)$ is non symmetric. This asymmetry is usually due to wind and surface tilt. Clearly using a Taylor expansion

$$\begin{aligned}(J * u^4)(x) - u^4 &= \int J(x-y)u^4(y)dy - u^4(x) \\ &= -(\int J(z)zdz)(u^4)'(x) + (\int J(z)z^2dz)(u^4)''(x) + ...\end{aligned}$$

If the kernel $J(.)$ is symmetric then

$$-(J * u^4 - u^4) \approx -(\int J(z)z^2dz)(4u^3u')'(x) \tag{5}$$

Thermal radiation is nearly always the dominant mode of heat transfer in the vicinity of a large fire source. Furthermore, it is usually accepted that radiation form the flames above the vegetable layer is not only the dominant radiative contribution, but also the main mechanism of fire spread [5]. The numerical treatment of radiation is computationally expensive since it is highly nonlinear and a three dimensional phenomena. So radiative models are restricted to approximated schemes. In this paper we present two simplified models for the thermal radiation: a local radiation diffusive model, and a non local radiation model.

Wind is an important hazard parameter in forest fire and thus a convenient local windfield should be generated. In the present examples the model developed in [6] is implemented.

2 Model with local radiation

In this first model we propose a simplified 2-D model where radiation is approximated by a non-linear diffusive term. The convective term takes into account the effect of the meteorological wind and the slope of the terrain. The non-dimensional equations are derived from the conservation law of energy and mass fraction using the Frank-Kamenetskii change of variables.

Let $Q = [0, l_x] \times [0, l_y] \subset \mathbb{R}^2$ a rectangle representing the projection of the surface where the fire takes place, big enough so the fire does not arrive to the boundary and

therefore Dirichlet boundary conditions can be considered.

$$\begin{aligned} \partial_t e + \mathbf{w} \cdot \nabla e - \nabla \left(K\left(u\right) \nabla u \right) + \alpha u = A f\left(u, y\right), \quad & \text{in } S \quad t \in (0, t_{max}), \\ e \in G(u), \quad & \text{in } S \quad t \in (0, t_{max}), \\ \partial_t y = -B f\left(u, y\right), \quad & \text{in } S \quad t \in (0, t_{max}), \end{aligned} \tag{6}$$

where again e is the non-dimensional enthalpy, u is the non-dimensional temperature and y is the non-dimensional mass fraction of fuel.

The non linear function $K\left(u\right) = \kappa \left(1 + \epsilon u\right)^3 + 1$, in the diffusive term represents the local radiation. The parameter K depends on the Stefan-Boltzmann constant, the optical path length for radiation, the thermal conductivity and the ambient temperature. The parameter ϵ depends on the activation energy, the universal constant of gases and the ambient temperature.

The function $f\left(u, y\right) = \left(u > u_{pc}\right) y \exp(u/(1 + \varepsilon u))$ is given by an Arrhenius type law where u_{pc} is the non dimensional temperature at which the process changes from endothermic to exothermic, and the logic expressions is equal to 1 if the expression is true and 0 if the expression is false. We write the pre-exponential factors A and B, out of the function f, in order to simplify notation. Notice that the pre-exponential factor B in 6 depends on the reaction heat.For more details about how to derive this model, its solution and applications see [7]

3 Model with non local radiation

Let S be a surface defined by the mapping

$$S: \ Q \longmapsto \mathbb{R}^3$$

$$x, y \longrightarrow (x, y, h(x, y))$$

representing the part of the terrain where the propagation of a fire can take place. We will assume that vegetation can be represented by a given fuel load together with a moisture content. Besides we will assume that the height of the flames in a particular fire are known and bounded by H. In order to take into account some three dimensional effects, and particularly the radiation from the flames above the surface S, we will consider the following three dimensional domain

$$D = \{(x, y, z) \in \mathbb{R}^3 \quad (x, y) \in Q, \quad h(x, y) < z < h(x, y) + H\}$$

This model considers the energy and mass conservation equations in the surface S, and the radiation equation in D.

$$\partial_t e + \alpha u = r \quad \text{in } S \quad t \in (0, t_{max}) \tag{7}$$

$$e \in G(u) \quad \text{in } S \quad t \in (0, t_{max}) \tag{8}$$

$$\partial_t y = -Bf(u, y), \quad \text{in } S \quad t \in (0, t_{max}), \tag{9}$$

Again the function f follows an Arrhenius type law
$f(u, y) = (u > u_p)(y > y_e)y \exp(-\gamma/(1 + u))$ where y_e is the mass fraction lower bound of extinction.

The right hand side of equation (7) describes the thermal radiation reaching the surface S from the flame above the layer. The intensity is defined as the radiation energy passing through an area per unit time, per unit of projected area and per unit of solid angle. The projected area is formed by taking the area that the energy is passing through and projecting it normal to the direction of travel. The unit elemental solid angle is centered about the direction of travel and has its origin at the area element.

After adimensionalization, the radiation equations in the direction Ω can be written as

$$\mathbf{\Omega}.\nabla i + a^* i = \delta(1 + u_g)^4 \quad \text{in } D \tag{10}$$

$$i = 0 \quad \text{on } \partial D \cap \{\mathbf{x};\ \mathbf{\Omega} \cdot \mathbf{n} < 0\} \tag{11}$$

where i is the non-dimensional radiation intensity, a^* is the non-dimensional absorbtion coefficient, u_g is the non dimensional flame temperature and δ depends on the Stefan-Boltzmann constant. The right hand side represents the total emissive power of a black-body. The incident energy at a point $\mathbf{x}(x, y, h(x, y))$ of the surface S due to radiation from the flame above the surface per unit time and per unit area will be obtained summing up the contribution of all directions $\mathbf{\Omega}$, that is

$$r(\mathbf{x}) = \int_{\omega=0}^{2\pi} i(\mathbf{x}, \mathbf{\Omega})\mathbf{\Omega} \cdot \mathbf{n}\, d\omega \tag{12}$$

where we have only considered the hemisphere above the fuel layer.

For more details about how derive this model, its solution and applications see [4].

4 Wind Field Model

4.1 Wind equations

Let $\omega \subset \mathbb{R}^2$ be a two–dimensional normalized bounded and connected domain representing the projection of the three–dimensional ground surface, $x = (x_1, x_2)$ be any of its points and τ be the time. We use small letters for the two–dimensional problem, and capital letters for the three–dimensional problem. All quantities are adimensionalised.

Let us consider the three–dimensional domain $\Omega = \{(x,z) : x \in \omega,\ h(x) < z < \delta\}$ representing the air layer studied. We assume that the height δ is small in front of the width and that the height $h(x)$ of the surface at point x is smaller than δ. In this section, we denote by an index $_{xz}$ the three–dimensional operators, and by an index $_x$ the bi-dimensional operators.

The air velocity $U = (U_1, U_2, U_3)$ and the potential P satisfy the Navier–Stokes equations. On one hand, the momentum equation reads

$$\frac{\partial U}{\partial \tau} + U \cdot \nabla_{xz} U - \frac{1}{Re}\Delta_{xz} U + \nabla_{xz} P = \frac{\lambda}{Re} T e_3, \tag{13}$$

where T is the adimensional temperature, Re is the Reynolds number, λ is related to the Grashoff number (indeed, λT is the Grashoff number), and $e_3 = (0,0,1)$.

On the other hand, the air compressibility is neglected, so that

$$\nabla_{xz} \cdot U = 0. \tag{14}$$

In order to specify the boundary conditions, we decompose the boundary into $\partial\Omega = S \cup A \cup L$, where $S = \{(x,z) : x \in \omega,\ z = h(x)\}$ is the ground surface, $A = \{(x,z) : x \in \omega,\ z = \delta\}$ is the air upper boundary and $L = \{(x,z) : x \in \partial\omega,\ h(x) < z < \delta\}$ is the air lateral boundary. Boundary conditions are

$$U \cdot N = 0, \quad \frac{\partial U}{\partial N}\Big|_{tan} = \zeta U, \quad \text{on } S, \tag{15}$$

$$U_3 = 0, \quad \partial_z U_1 = \partial_z U_2 = 0, \quad \text{on } A, \tag{16}$$

$$U|_L = (v_m, 0), \quad \text{on} L, \tag{17}$$

where ζ is the friction coefficient, N is the 3D inner unit normal vector field to $\partial\Omega$, and the subscript $_{tan}$ denotes the tangential component. Here v_m is the horizontal component of the meteorological wind (its vertical component is neglected), that is assumed to be known, non depending on z and with a null total flux through the lateral boundary, that is,

$$\partial_z v_m = 0, \quad \int_{\partial\omega} (\delta - h)\, v_m \cdot \nu \, ds = 0, \tag{18}$$

where $\nu = (\nu_1, \nu_2)$ is the 2D inner unit normal vector field to $\partial\omega$. We complete these equations with the initial condition

$$U|_{\tau=0} = U_0, \tag{19}$$

where U_0 is the initial velocity, that we assume to be known. Equations (13) to (19) are well posed, *i.e.* there exists a solution (U, P), which is unique up to an additive constant on pressure for a small enough Reynolds number.

We distinguish the vertical velocity from the horizontal one denoting $W = U_3$, $V = (U_1, U_2)$, and we define the horizontal flux at a point $x \in \omega$ and time τ by

$$\overline{V}(\tau, x) = \int_{h(x)}^{\delta} V(\tau, x, z)\, dz. \tag{20}$$

The incompressibility and the fact that the air does neither cross S nor A, that is, $U \cdot N = 0$, involve that the horizontal flux is also incompressible, that is

$$\nabla_x \cdot \overline{V} = 0. \tag{21}$$

4.2 Asymptotic wind equations

Using the fact that the thickness δ of the considered air layer is small compared with its width, and assuming that the wind is not too strong and more precisely that $\delta^2 Re \ll 1$, then preserving only the dominant terms and re-scaling P, Equations (13) and (14) write

$$\begin{aligned} -\partial^2_{zz} V + \nabla_x P &= 0, & (22)\\ \partial_z P &= \lambda T, & (23)\\ \nabla_x \cdot V + \partial_z W &= 0. & (24) \end{aligned}$$

Boundary conditions (15), (16) and (17) give

$$\begin{aligned} (V, W) \cdot N = 0, \quad \partial_z V = \zeta V, \quad &\text{on } S, & (25)\\ W = 0, \quad \partial_z V = 0, \quad &\text{on } A, & (26)\\ \overline{V} \cdot \nu = (\delta - h) v_m \cdot \nu, \quad &\text{on } \partial\omega. & (27) \end{aligned}$$

Equations (22) to (27) are well posed: given v_m satisfying (18) and T, there exists a solution (V, W, P) which is unique up to an additive constant on P. For more details about this convection asymptotic model and its further solution (28), (29) and (30), see [6].

4.3 3D Horizontal velocity in terms of 2D potential

We assume that the air temperature linearly decreases with the height and vanishes on the upper boundary (for a non zero constant given air temperature on the upper boundary, similar formulas hold and numerical results are very close), that is

$$T(\tau, x, z) = t_S(\tau, x) \frac{\delta - z}{\delta - h(x)},$$

and that the temperature $t_S = t_S(\tau, x)$ on ground surface is given. Then, by Equation (23), there exists a 2D potential $p = p(\tau, x)$ such that

$$P(\tau, x, z) = p(\tau, x) + t(\tau, x)\Big(\delta z - \frac{1}{2} z^2\Big),$$

where t is a re-scaled temperature given by

$$t(\tau, x) = \frac{\lambda t_S(\tau, x)}{\delta - h(x)}.$$

The potential p is called 2D because it only depends on the first two spaces variables $x = (x_1, x_2)$; it also depends on time τ, but this last acts now as a parameter.

Then, Equation (22) and boundary conditions $\partial_z V(\tau, x, \delta) = 0$ and $\partial_z V(\tau, x, h(x)) = \zeta V(\tau, x, h(x))$ included in (26) and (25) provide

$$V(x, z) = m(x, z)\nabla_x p(\tau, x) + n(x, z)\nabla_x t(\tau, x), \tag{28}$$

where

$$\begin{aligned} m(x,z) &= \Big(\frac{1}{2}z^2 - \delta z - \frac{1}{2}h^2(x) + (\delta+\xi)h(x) - \xi\delta\Big), \\ n(x,z) &= \Big(-\frac{1}{24}z^4 + \frac{1}{6}\delta z^3 - \frac{1}{3}\delta^3 z + \frac{1}{24}h^4(x) - \frac{1}{6}(\delta+\xi)h^3(x) \\ &\quad + \frac{1}{2}\xi\delta h^2(x) + \frac{1}{3}\delta^3 h(x) - \frac{1}{3}\xi\delta^3\Big), \end{aligned}$$

being $\xi = 1/\zeta$ the inverse of the friction coefficient ζ.

4.4 Equations governing the 2D potential

Using (28) in Equations (21) (which follows from (24), (25) and (26)) and (27), we find that the potential $p = p(\tau, x)$ satisfies the following 2D boundary problem

$$-\nabla_x \cdot (a\nabla_x p) = \nabla_x \cdot (b\nabla_x t) \quad \text{in } \omega, \tag{29}$$

$$a\frac{\partial p}{\partial \nu} = -b\frac{\partial t}{\partial \nu} + v \quad \text{on } \partial\omega, \tag{30}$$

where

$$a = a(x) = \frac{1}{3}(\delta - h(x))^2(3\xi + \delta - h(x)),$$

$$b = b(x) = \frac{1}{30}(\delta - h(x))^2\Big(2\delta^2(2\delta + 5\xi) - 2\delta(\delta - 5\xi)h(x) - (3\delta + 5\xi)h^2(x) + h^3(x)\Big),$$

and

$$v = v(\tau, x) = (\delta - h(x))v_m(\tau, x) \cdot \nu(x)$$

is the horizontal normal flux on $\partial\omega$. By Hypothesis (18), it satisfies

$$\int_{\partial\omega} v = 0. \tag{31}$$

Equations (29)–(30) are well posed: given t and v, there exists a solution p, which is unique up to an additive constant. This constant will be fixed by the extra condition

$$\int_\omega p = 0.$$

4.5 Variational solution of the 2D potential equations

Let

$$L_0^2(\partial\omega) = \Big\{ v \in L^2(\partial\omega) : \int_{\partial\omega} v = 0 \Big\},$$
$$\mathcal{V} = \Big\{ \varphi \in H^1(\omega) : \int_{\omega} \varphi = 0 \Big\}.$$

Given $t \in H^1(\omega)$ and $v \in L_0^2(\partial\omega)$, by Lax–Milgram theorem, there exists a unique $p \in \mathcal{V}$ such that

$$\int_\omega a\nabla p \cdot \nabla\varphi = \int_{\partial\omega} v\varphi - \int_\omega b\nabla t \cdot \nabla\varphi, \quad \forall \varphi \in \mathcal{V}. \tag{32}$$

Let us check that it satisfies (29) and (30). Given $\phi \in \mathcal{D}(\omega)$, $\varphi = \phi + c$ belongs to $\mathcal{V}$ for some $c \in \mathbb{R}$; then (32) writes $\int_\omega a\nabla p \cdot \nabla\phi = -\int_\omega b\nabla t \cdot \nabla\phi$ since $\int_{\partial\omega} v(\phi + c) = c\int_{\partial\omega} v = 0$. This provides Equation (29) in distribution sense. Now (29) and (32) give $\int_\omega (\nabla \cdot (a\nabla p + b\nabla t))\varphi = \int_{\partial\omega} v\varphi$. This provides Boundary Condition (30) in a weak sense since φ may coincide with any given element of $H^1(\omega)$ in a neighborhood of $\partial\omega$.

In fact, data depend on time τ which acts as a parameter: given $t(\tau) \in H^1(\omega)$ and $v(\tau) \in L_0^2(\partial\omega)$, there exists a unique solution $p(\tau) \in \mathcal{V}$.

5 The Optimal Control Problem

In order to simplify notation in the sequel, the time τ is omitted since it acts as a parameter, and the index $_x$ is omitted in differential operators since they only act on this variable.

5.1 Identification of wind on the boundary

We are going now to identify v to the solution u of an optimal control problem: given N experimental measurements V_i of the wind velocity at given points (x_i, z_i), $i = 1,\dots N$, we search the value of $v \in L_0^2(\partial\omega)$ such that the $V(x_i, z_i)$ given by (28) are as close as posible to the experimental values V_i. This is an optimal control problem where:

- $v \in L_0^2(\partial\omega)$ is the control.
- The state equations is (32).
- The cost function is chosen to be

$$J(v) = \frac{1}{2}\sum_{i=1}^{N} \|V(x_i, z_i) - V_i\|^2 + \frac{\alpha}{2}\int_{\partial\omega} v^2.$$

Due to (28),

$$J(v) = \frac{1}{2}\sum_{i=1}^{N} \|m(x_i, z_i)\nabla p(x_i) + n(x_i, z_i)\nabla t(x_i) - V_i\|^2 + \frac{\alpha}{2}\int_{\partial\omega} v^2. \tag{33}$$

In practice, instead of (33), we use the following regularized functional

$$J(v) = \frac{1}{2}\sum_{i=1}^{N} \int_{\omega} \rho_{\epsilon,i}(x)\|m(x, z_i)\nabla p(x) + n(x, z_i)\nabla t(x) - V_i\|^2\, dx + \frac{\alpha}{2}\int_{\partial\omega} v^2 \tag{34}$$

where $\rho_{\epsilon,i}$ is a suitable mollifier cancelling outside a small ball $B(x_i, \epsilon)$ and such that $\int \rho_{\epsilon,i}(x)\, dx = 1$. For example,

$$\rho_{\epsilon,i}(x) = \frac{1}{\epsilon^2}\rho\Big(\frac{x - x_i}{\epsilon}\Big),$$

where $\rho(x) = c\exp(-1/(1 - ||x||^2))$ for $||x|| < 1$, and $\rho(x) = 0$ for $||x|| \geq 1$.

The optimal control problem to be solved is to find $u \in L_0^2(\partial\omega)$ such that

$$J(u) = \inf_{v \in L_0^2(\partial\omega)} J(v). \tag{35}$$

Remark. The regularization term $\frac{\alpha}{2}\int_{\partial\omega} v^2 d\sigma$ is necessary for mathematical reasons. Indeed, without this term the optimal control problem has no solution (if we search for the control u in the whole space L_0^2). We have choosen α a small number. If a good estimation of the wind flux $v \approx u^*$ is known on the boundary, we can modify the cost functional in (33) as follows:

$$J(v) = \frac{1}{2}\sum_{i=1}^{N} \int_{\omega} \rho_{\epsilon,i}(x)\|m(x, z_i)\nabla p(x) + n(x, z_i)\nabla t(x) - V_i\|^2\, dx + \frac{\alpha}{2}\int_{\partial\omega} (v - u^*)^2 d\sigma \tag{36}$$

and choose a larger value for α. Note that we cannot impose at the same time the value of the wind flux on the boundary and the value of the solution at several given points, as once the wind flux v is given on the boundary the wind field is uniquely determined by (29)-(30). Therefore the optimal control problem with the former functional is a compromise (and so is the value of the parameter α) between these two sets of data. Usually in practical applications we do not have a good estimation of the flux on the boundary, and this is the reason why we choose the value of α to be small, typically $\alpha = 0.001$.

5.2 Solution of the optimal control problem

Let $Bv \in \mathcal{V}$ be the solution of

$$\int_{\omega} a\nabla Bv \cdot \nabla\varphi = \int_{\partial\omega} v\varphi, \quad \forall\varphi \in \mathcal{V}, \tag{37}$$

and $r \in \mathcal{V}$ be the solution of

$$\int_\omega a\nabla r \cdot \nabla\varphi = -\int_\omega b\nabla t \cdot \nabla\varphi, \quad \forall\varphi \in \mathcal{V}. \tag{38}$$

The operator B is linear continuous from $L_0^2(\partial\omega)$ in $\mathcal{V}$, and r is independent of v.

The solution of (32) is $p = Bv + r$, therefore

$$J(v) = \frac{1}{2}\pi(v,v) - \lambda(v) + \mu \tag{39}$$

where π is the bilinear continuous function on $L_0^2(\partial\omega) \times L_0^2(\partial\omega)$ given by

$$\pi(u,v) = \sum_{i=1}^{N} \int_\omega \rho_{\epsilon,i}(m\nabla Bu) \cdot (m\nabla Bv) + \alpha \int_{\partial\omega} uv, \tag{40}$$

λ is the continuous linear function in $L_0^2(\partial\omega)$ given by

$$\lambda(v) = \sum_{i=1}^{N} \int_\omega \rho_{\epsilon,i}(m\nabla r + n\nabla t - V_i) \cdot m\nabla Bv, \tag{41}$$

and μ is the constant

$$\mu = \frac{1}{2}\sum_{i=1}^{N} \int_\omega \rho_{\epsilon,i} V_i \cdot V_i. \tag{42}$$

Obviously,

$$\pi(v,v) \geq \alpha ||v||^2_{L_0^2(\partial\omega)}.$$

Then, by Theorem 1.1 Chapter 1 in [9], there exist a unique solution u of Problem (35). It is characterized by $J'(u) = 0$, where $J'(u)$ is the derivative of J at point u, which is a real linear continuous function on $L_0^2(\partial\omega)$. That is

$$J'(u) \cdot v = 0, \quad \forall v \in L_0^2(\partial\omega). \tag{43}$$

Using the chain rule,

$$J'(u) \cdot v = \sum_{i=1}^{N} \int_\omega \rho_{\epsilon,i}(m\nabla p + n\nabla t - V_i) \cdot m\nabla Bv + \alpha \int_{\partial\omega} uv \tag{44}$$

(this formula holds for all $u \in \mathcal{V}$).

5.3 Definition of the adjoint state and elimination of the control

Denote now p the potential associated to u by (32), that is the unique solution $p \in \mathcal{V}$ of

$$\int_\omega a\nabla p \cdot \nabla\varphi = \int_{\partial\omega} u\varphi - \int_\omega b\nabla t \cdot \nabla\varphi, \quad \forall\varphi \in \mathcal{V}. \tag{45}$$

Let

$$\mathcal{W} = \Big\{\psi \in H^1(\omega) : \int_{\partial\omega} \psi = 0\Big\}.$$

We introduce the adjoint state as the solution $q \in \mathcal{W}$ of:

$$\int_\omega a\nabla q \cdot \nabla \psi = \sum_{i=1}^{N} \int_\omega \rho_{\epsilon,i}(m\nabla p + n\nabla t - V_i) \cdot m\nabla \psi, \quad \forall \psi \in \mathcal{W}. \tag{46}$$

Since $J'(u) = 0$ the expression (44) of J' provides

$$\sum_{i=1}^{N} \int_\omega \rho_{\epsilon,i}(m\nabla p + n\nabla t - V_i) \cdot m\nabla Bv = -\alpha \int_{\partial\omega} uv. \tag{47}$$

Let us take $\psi = Bv + c$ in (46) where $c = -\int_{\partial\omega} Bv/|\omega|$ is such that $\psi \in \mathcal{W}$. With (47) it gives

$$\int_\omega a\nabla q \cdot \nabla Bv = -\alpha \int_{\partial\omega} uv. \tag{48}$$

On the other hand, let us take $\varphi = q + c'$ in Definition (37) of Bv, where $c' = -\int_\omega q/|\omega|$ is such that $\varphi \in \mathcal{V}$. Since $\int_{\partial\omega} v = 0$, we get

$$\int_\omega a\nabla Bv \cdot \nabla q = \int_{\partial\omega} vq + c' \int_{\partial\omega} v = \int_{\partial\omega} vq. \tag{49}$$

Comparing (48) and (49), it results, for all $v \in L^2_0(\partial\omega)$,

$$\int_{\partial\omega} qv = -\alpha \int_{\partial\omega} uv. \tag{50}$$

Since $u \in L^2_0(\partial\omega)$ (by definition (35)) and $q|_{\partial\omega} \in L^2_0(\partial\omega)$ (because $\int_{\partial\omega} q = 0$ from $q \in \mathcal{W}$), (50) implies

$$u = -\frac{1}{\alpha} q. \tag{51}$$

Using this, Definition (45) of p, gives

$$\int_\omega a\nabla p \cdot \nabla \varphi + \frac{1}{\alpha} \int_{\partial\omega} q\varphi = -\int_\omega b\nabla t \cdot \nabla \varphi, \quad \forall \varphi \in \mathcal{V}. \tag{52}$$

5.4 An equivalent problem

In order to allow easier numerical computation, let us see that it is equivalent to solve coupled equations (52) and (46) in $H^1(\omega)$ instead of $\mathcal{V}$ and $\mathcal{W}$.

On one hand, $(p, q) \in H^1(\omega) \times H^1(\omega)$ and satisfies

$$\int_\omega a\nabla p \cdot \nabla \varphi + \frac{1}{\alpha} \int_{\partial\omega} q\varphi = -\int_\omega b\nabla t \cdot \nabla \varphi, \quad \forall \varphi \in H^1(\omega), \tag{53}$$

$$\int_\omega a\nabla q \cdot \nabla \psi = \sum_{i=1}^{N} \int_\omega \rho_{\epsilon,i}(m\nabla p + n\nabla t - V_i) \cdot m\nabla \psi, \quad \forall \psi \in H^1(\omega). \tag{54}$$

Indeed (53) is satisfied by constant φ (since $\int_{\partial\omega} q = 0$) and therefore by all $\varphi' + c$ with $\varphi' \in \mathcal{V}$ and $c \in \mathbb{R}$, that is for all $\varphi \in H^1(\omega)$. And (54) is satisfied by constant ψ and therefore by all $\psi' + c$ with $\psi' \in \mathcal{W}$, that is for all $\psi \in H^1(\omega)$.

On the other hand, let us check that the solution of (53)–(54) is unique up to a constant on p. Let here (p, q) denote the difference of two possible solutions. It satisfies (53)–(54) with $t = 0$ and $V_i = 0$. Setting $\varphi = q$ in such (53) and $\psi = -p$ in such (54) and adding, we get

$$\frac{1}{\alpha}\int_{\partial\omega} q^2 + \sum_{i=1}^{N}\int_{\omega} \rho_{\epsilon,i}\|m\nabla p\|^2 = 0$$

and then $q|_{\partial\omega} = 0$. Setting now $\varphi = p$ in (53), we get $\int_\omega a\|\nabla p\|^2 = 0$ and then $\nabla p = 0$ and p is constant. Setting finally $\psi = q$ in (54), we get $\int_\omega a\|\nabla q\|^2 = 0$ and then $q|_{\partial\omega} = 0$ gives $q = 0$. This proves that $(\nabla p, q)$ is unique, that is the uniqueness of (p, q) up to a constant on p.

5.5 Expression of the adjusted wind

There exists a unique $(\nabla p, q)$ solution of coupled equations (53)–(54). Indeed there exists $u \in L^2_0(\partial\omega)$ satisfying (43), and then $p \in \mathcal{V}$ solution of (45) and $q \in \mathcal{W}$ solution of (46), and then $(\nabla p, q)$ satisfies (53)–(54) and is unique as seen in section 5.4. The adjusted wind velocity $V(x, z)$ is given in terms of this $\nabla p(x)$ at every point (x, z) by (28).

6 Approximated Solution

6.1 Approximated equations

In order to make p unique and to improve numerical solution, we actually compute the solution of the following approximated equations: find $(p, q) \in H^1(\omega) \times H^1(\omega)$ solution of

$$\int_\omega a\nabla p\cdot\nabla\varphi + \eta\int_{\partial\omega} p\varphi + \frac{1}{\alpha}\int_{\partial\omega} q\varphi = -\int_\omega b\nabla t\cdot\nabla\varphi, \quad \forall\varphi\in H^1(\omega), \tag{55}$$

$$\int_\omega a\nabla q\cdot\nabla\psi + \eta\int_{\partial\omega} q\psi = \sum_{i=1}^{N}\int_\omega \rho_{\epsilon,i}(m\nabla p + n\nabla t - V_i)\cdot m\nabla\psi, \quad \forall\psi\in H^1(\omega), \tag{56}$$

for a small parameter η (in the examples below $\eta = 0.001$), and then we compute the (approximated ajusted) wind velocity $V(x, z)$ at every point (x, z) in terms of $\nabla p(x)$ using expression (28).

Remark. The reader could expect regularization terms involving integrals on ω instead of $\partial\omega$. In (56), the regularization term $\eta\int_{\partial\omega} q\psi$ is used in order to get $\int_{\partial\omega} q = 0$ (by choosing $\psi = 1$). Indeed this important condition (it gives $u \in L^2_0(\partial\omega)$ by (51)) which followed from the exact equation (53) (by choosing $\varphi = 1$) is no longer contained in the approximated equation (55). In this last, we then use the regularization term $\eta\int_{\partial\omega} p\varphi$ in order to get Equality (57) below.

6.2 Convergence

Let us check that the solution of (55)–(56) goes to the solution of exact equations (53)–(54) as $\eta \to 0$. At first, let us bound q. Setting $\varphi = q$ in (55), $\psi = -p$ in (56) and adding, we get

$$\frac{1}{\alpha}\int_{\partial\omega} q^2 + \sum_{i=1}^{N}\int_{\omega} \rho_{\epsilon,i}\|m\nabla p\|^2 = -\int_{\omega} b\nabla t\cdot\nabla q - \sum_{i=1}^{N}\int_{\omega}\rho_{\epsilon,i}(n\nabla t - V_i)\cdot m\nabla p. \tag{57}$$

By Cauchy–Schwarz inequality, it follows that

$$\frac{1}{\alpha}\int_{\partial\omega} q^2 + \frac{1}{2}\sum_{i=1}^{N}\int_{\omega} \rho_{\epsilon,i}\|m\nabla p\|^2 \le c_1 - \int_{\omega} b\nabla t\cdot\nabla q. \tag{58}$$

Here and in the sequel, c_i denotes various positive numbers independent of η, p and q. Setting $\psi = q$ in (56) and using $m \le c_2 a$ and Cauchy–Schwarz inequality, we get

$$\frac{1}{2}\int_{\omega} a\|\nabla q\|^2 + \eta\int_{\partial\omega} q^2 \le c_3\sum_{i=1}^{N}\int_{\omega}\rho_{\epsilon,i}\|m\nabla p\|^2 + c_4. \tag{59}$$

Dividing by $2c_3$, adding to (58) and using $b \le c_5 a$ and Cauchy–Schwarz inequality, we get

$$\frac{1}{\alpha}\int_{\partial\omega} q^2 + c_6\int_{\omega} a\|\nabla q\|^2 \le c_7. \tag{60}$$

This implies that q is bounded in $H^1(\omega)$.

Now, let us bound p. Setting $\varphi = p$ in (55) and using $b \le c_5 a$, Cauchy–Schwarz inequality and (60), we get

$$\frac{1}{2}\int_{\omega} a\|\nabla p\|^2 + \eta\int_{\partial\omega} p^2 \le c_8 - \frac{1}{\alpha}\int_{\partial\omega} pq \le c_8 + c_9\Big(\int_{\partial\omega} p^2\Big)^{1/2}. \tag{61}$$

Setting $\psi = 1$ in (56), we get $\int_{\partial\omega} q = 0$, and then, setting $\varphi = 1$ in (55), we get

$$\int_{\partial\omega} p = -\frac{1}{\alpha\eta}\int_{\partial\omega} q = 0. \tag{62}$$

Therefore Poincaré–Wirtinger inequality $(\int_{\partial\omega} p^2)^{1/2} \le c_{10}(\int_{\omega}\|\nabla p\|^2)^{1/2}$ holds. Then (61) gives $(\int_{\omega}\|\nabla p\|^2)^{1/2} \le c_{11}$ and p is bounded in $H^1(\omega)$.

Let now $\eta_n \to 0$. There exists a subsequence such that the corresponding solution (p_n, q_n) of (55)–(56) goes to some limit (p, q) weakly in $H^1(\omega)\times H^1(\omega)$ and therefore strongly in $L^2(\omega)\times L^2(\omega)$ and its trace converges strongly in $L^2(\partial\omega)\times L^2(\partial\omega)$. Then the limit (p, q) satisfies exact equations (53)–(54). These equations possessing a unique solution, as seen in § 5.4, all subsequences go to the same limit and therefore the whole sequence (p_n, q_n) goes to (p, q).

6.3 Computation of wind

Practically, we compute the unique solution (p, q) of (approximated) coupled equations (55)–(56) for a small parameter η, and then we compute the (approximated ajusted) wind velocity $V(x, z)$ at every point (x, z) in terms of $\nabla p(x)$ using expression (28).

6.4 Finite element approximation

Let us discretize the approximated equations (55)–(56). Let $\mathcal{T}_H$ be a uniform triangulation of ω corresponding to a discretization parameter H and let V_H be the associated space of P_1 (or P_2) finite elements. Besides a better order of convergence, a reason in favor of P_2 against P_1 is that in practical applications, the variable of physical interest is the wind velocity V which is obtained from the potential p using expression (28), involving derivatives.

Choosing a finite element basis $\{\phi_i\}$ for V_H, we introduce the following matrices

$$G = \left\{ \int_\omega a\, \nabla\phi_r \cdot \nabla\phi_k + \eta \int_{\partial\omega} \phi_r \phi_k \right\}_{r,k},$$

$$C_1 = \left\{ \frac{1}{\alpha} \int_{\partial\omega} \phi_r \phi_k \right\}_{r,k}, \quad C_2 = \left\{ \sum_{i=1}^{N} \int_\omega \rho_{\epsilon,i}\, m^2\, \nabla\phi_r \cdot \nabla\phi_k \right\}_{r,k}$$

and the vectors

$$f_p = \left\{ -\int_\omega b \nabla t \cdot \nabla\phi_r \right\}_r, \quad f_q = \left\{ -\sum_{i=1}^{N} \int_\omega \rho_{\epsilon,i}(n\nabla t - V_i) m \cdot \nabla\phi_r \right\}_r.$$

Then, the discrete problem associated to (55)–(56) is the following linear algebraic system:

$$\begin{bmatrix} G & C_1 \\ -C_2 & G \end{bmatrix} \begin{bmatrix} p \\ q \end{bmatrix} = \begin{bmatrix} f_p \\ f_q \end{bmatrix} \tag{63}$$

The matrix in (63) being nonsymmetric and very ill-conditioned, most of the standard iterative methods fail to converge or have a very slow convergence (this is the case of GMRES-ILU preconditioned). For moderate number of unknowns we use the state-of-the-art sparse LU factorization [10]. In [11] a highly effective solution method is obtained by means of a preconditioned Schur complement approximate, leading to a nonsymmetric system that can be solved by GMRES in a constant number of iterations. For the description and a complete numerical analysis of this approximate see [11]. According to this numerical analysis and to the numerical experiments described in the following section, the number of iterations appears to be insensitive to η and only mildly dependent on α. Note that p is determined up to a constant, but only ∇p is needed to compute the wind velocity V. Then we choose η small enough so that the perturbation term does not affect the value of ∇p up to the desired precision.

7 Numerical Examples

7.1 Example 1: Wind filed adjustement with real data

We have considered a simulation using realistic wind data that have been supplied by *Desarrollos Eólicos S.A., (DESA)* in several measurement points for an episode along March 21, 2003, see [12].

The studied three-dimensional domain Ω is located near Lugo, Spain, at $43N$ of latitude and it is horizontally limited by four points of UTM coordinates (609980, 4799020), (626000,4799020), (626000, 4813040) and (609980, 4813040), respectively. The upper boundary A of Ω has been taken at a height $\delta = 1080\ m$. A digital elevation map was provided by *DESA* on a quadrilateral grid of element size $20 \times 20\ m$. The X axis corresponds to East direction and the Y one to North. Thus, we are working with a region of $16020 \times 14020\ m$. The minimum and maximum terrain heights are $420\ m$ and $1020\ m$, respectively. Figure 1 represents a color map of the heights of the terrain.

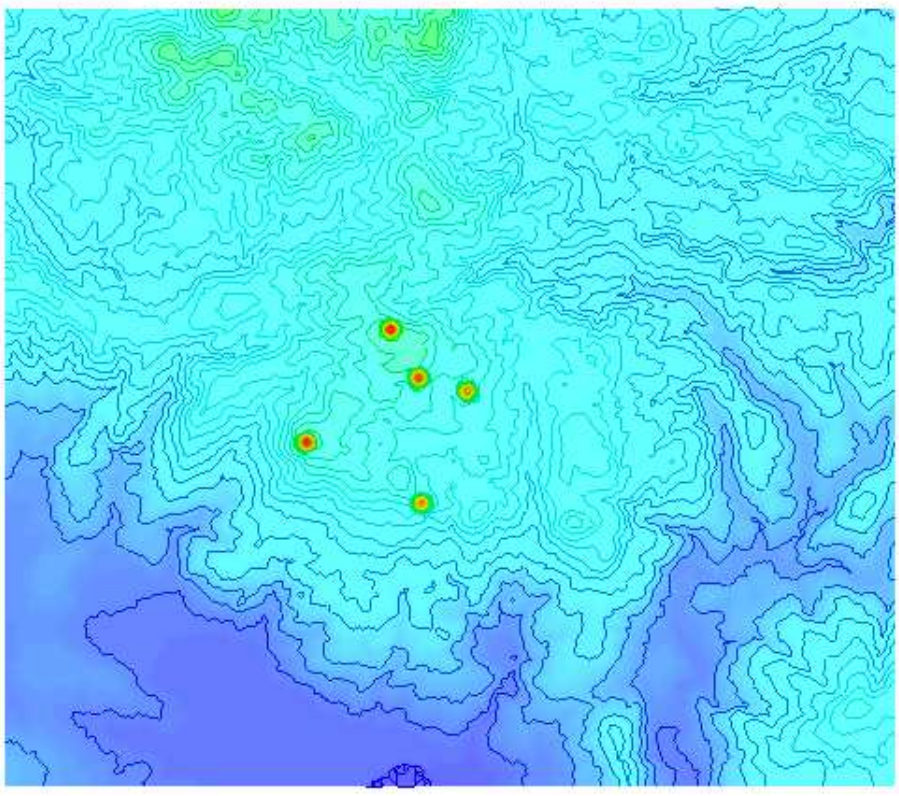

Figure 1.— Terrain heights and stations: From North to South E208, E212, E242, E206 and E283

Wind has been measured every 10 minute at 5 stations which are plotted on Figure 1: from North to South, we find E208, E212, E242, E206 and E283. At stations E208 and E212, the wind was measured at two different heigts. Their coordinates are given in Table 1.

Station	UTM-E	UTM-N	Height
E206	615396	4805218	924.8
E208	616917	4807256	945.0
E212	617423	4806382	895.0
E242	618290	4806136	873.2
E283	617473	4804111	849.0

Table 1.— Coordinates of stations (in meters)

Roughness is an essential factor on the characteristics of the resulting wind profile. In this case, the roughness length values are 0.03 m, 0.05 m, 0.08 m, 0.3 m and 0.8 m.

7.1.1 Wind computation for above real data

We procede in three steps:

- First, we estimate the main parameters of our optimal control wind model.
- We compute the wind with our model using data of *input stations* E206, E208 and E212.
- Finally, we compare the computed wind to the measured wind at *control stations* E242 and E283 (Table 2). They are also compared at input stations (Table 3) but this is less significant since, there, the computed wind is optimized to be close to data.

We propose a quadratic adjustment of the friction coefficient in terms of the of the roughness of the terrain, i.e., $\zeta = a_0 + a_1 z_0 + a_2 z_0^2$. We have used a standard genetic algorithm code (*pgapack* library), with string real coding, based on the model developed by Levine [13] to look for optimal values of these quadratic adjustment parameters $a_0\,, a_1$ and a_2. We search for the optimum of the linear parameter a_0 in $[1, 10]$, the first order parameter a_1 in $[0, 5]$ and the second order parameter a_2 in $[-0.05, 0.05]$. The values of the coefficients a_i depends slightly of the meteorological conditions, which means that the friction coefficient depends slightly on the solution. Typical values of the coefficients are $a_0 = 3$, $a_1 = 0.5$ and $a_0 = -0.01$ showing in practice a linear dependence of the friction coefficient with the roughness.

We have computed the wind every 10 minutes throughout the day with our optimal control model for the above adjusted parameters, using wind data only at stations E206, E208 and E212 (*input stations*). The data at the two other stations, E242 and E283 (*control stations*), are not used as input; they are used to control the efficiency of our model. The measured and the computed wind velocities at these control stations are shown in Figures 2 and 3. The estimation of the parameters a_i has been carried out only once each hour (24 computations along the day) using the first experimental wind measurements that are available at the begining of each hour.

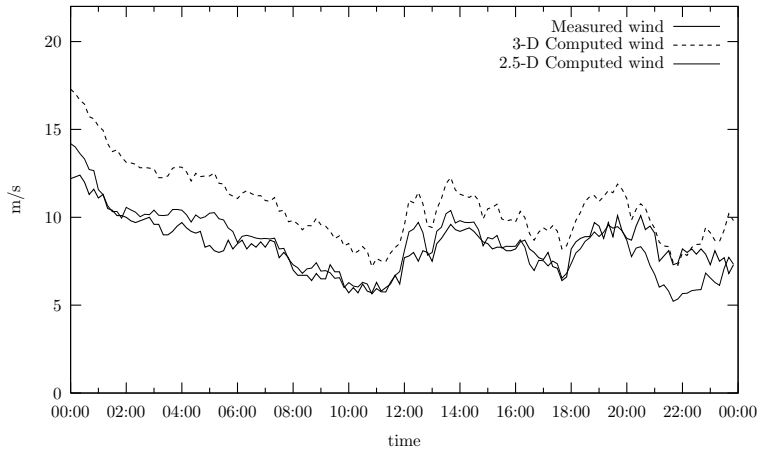

Figure 2.— Comparison of measured and computed wind velocities at control station E242

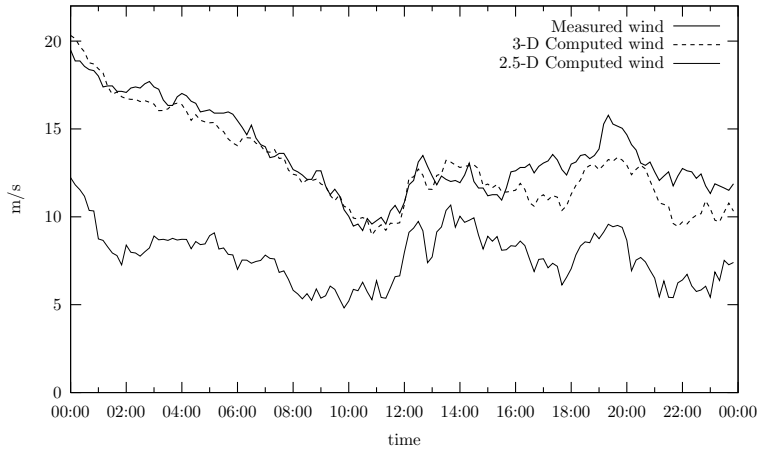

Figure 3.— Comparison of measured and computed wind velocities at control station E283

In order to compare our model (called 2.5-D model) with classical wind adjustment models, these figures include the wind velocities computed by the three-dimensional mass consistent model (3-D model) described in [12].

Errors of the computed winds with respect to the measured winds at control stations are given in Table 2. Remark that the present 2.5-D model provides better results at the control station E242 which is close to the input stations (see Figure 1). On the contrary, the 3-D model is more accurate at the control station E283 which is far from the input stations. This error can be explained by the fact that the hypothesis of the 2.5-D model are broken by the more rugged terrain at the station E283 (we can see on Figure 1 that the level set lines are streched close to E283).

Stations and control points	Average measured wind	Average computed wind	% average error	Maximum absolute error	Minimum absolute error	Model
E242 (40 m)	8.40	10.69	27.24%	5.09	0.09	3-D
	8.40	8.49	1.05 %	2.54	0.01	2.5-D
E283 (49 m)	13.62	12.95	4.94 %	3.04	0.02	3-D
	13.62	7.73	43.28 %	9.88	1.34	2.5-D

Table 2.— Error at control stations

Errors at input stations are given in Table 3. As expected, average errors are small.

Stations and control points	Average measured wind	Average computed wind	% average error	Maximum absolute error	Minimum absolute error	Model
E206 (49 m)	15.37	15.50	0.81 %	0.46	0.01	3-D
	15.37	14.82	3.62 %	1.15	0.23	2.5-D
E208 (15 m)	8.57	8.98	4.74 %	1.25	0.00	3-D
	8.57	9.13	6.52 %	2.45	0.01	2.5-D
E208 (30 m)	9.25	9.92	7.21 %	1.36	0.05	3-D
	9.25	9.42	1.82 %	1.41	0.00	2.5-D
E212 (15 m)	8.46	8.44	0.20 %	0.63	0.00	3-D
	8.46	8.18	3.33 %	1.89	0.01	2.5-D
E212 (30 m)	9.02	9.85	9.25 %	1.60	0.31	3-D
	9.02	8.46	6.17 %	2.16	0.01	2.5-D

Table 3.— Error at input stations

7.2 Example 2: Fire propagation in the Ebro River Basin

In this example we consider the fire propagation in a zone of the Ebro river basin where the combined effects of the topography, wind and radiation can be observed. First due to the wind the fire front follows teh riverbed. Later the wind turns and by effect of radiation the fire cross the river and rises up to the top of the mountain.

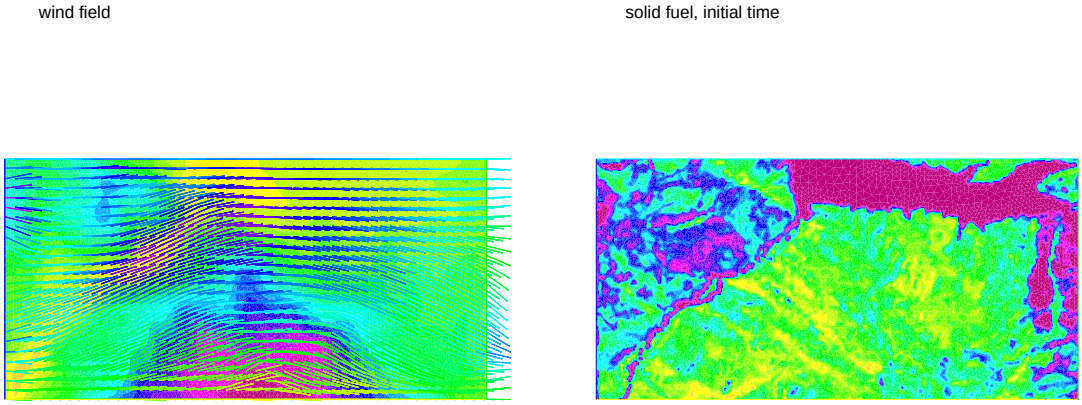

Figure 4.— Wind field, topography and initial fuel distribution

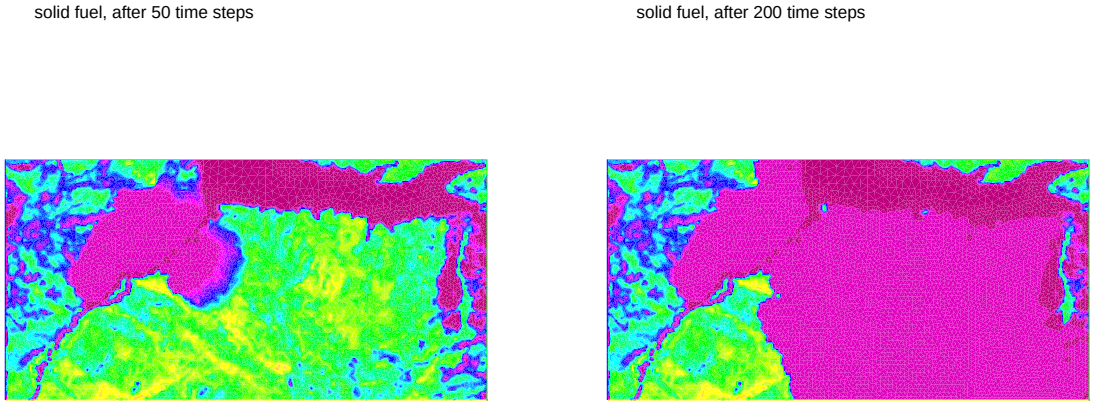

Figure 5.— Fuel distribution and burned zone after 50 and 200 time steps

References

[1] R.C. Rothermel. A mathematical model for predicting fire spread in wildland fuels. *General Technical Report INT-115, USDA Forest Service, Intermountain Forest and Range Experiment Station, 1972.*

[2] Margerit J, Séro Guillaume O. *Modelling forest fires. Part II: reduction to two-dimensional models and simulation of propagation.* Int. J. Heat and Mass Transfer 45, 1723-1737, 2002.

[3] Margerit J, Séro Guillaume O. *Modelling forest fires. Part I: A complete set of equations derived by extended irreversible thermodynamics.* Int. J. Heat and Mass Transfer 45, 1723-1737, 2002.

[4] L. Ferragut, M.I. Asensio, S. Monedero. *Modelling radiation and moisture content in fire spread.* Communications in Numerical Methods in Engineering 23, 819-833, 2007.

[5] Cox G. *Combustion Fundamentals of Fire.* Academic Press, London, 1995.

[6] M.I. Asensio, L. Ferragut, J. Simon, *A convection model for fire spread simulation*, Applied Mathematics Letters 18, 673-677, 2005.

[7] M. I Asensio, L. Ferragut. *On a wildland fire model with radiation* Int. J. Num. Methods Eng. 54, 137-157, 2002.

[8] Ferragut L., Asensio M.I., Simon, J. High Definition local adjustment model of 3D Wind Fields performing only 2D computations. *Commun. Numer. Meth. Eng.*, D.O.I:10.1002/cnm.1314, 2009.

[9] Lions J.-L., *Optimal control of sytems governed by partial differential equations.* Springer, Berlin, 1971.

[10] Davis T.A., *Direct Methods for Sparse Linear Systems.* SIAM, Philadelphia, 2006.

[11] Benzi M., Ferragut L., Pennacchio M., Simoncini V., Solution of Linear Systems from an Optimal Control Problem Arising in Wind Simulation. *Numer. Linear Algebra Appl.*, in press, 2009.

[12] Montenegro R., Montero G., Rodriguez E., Escobar J.M., González-Yuste J.M., Applications of genetic algorithms in realistic wind field simulations. *Studies in Comp Intelligence*, **102** (2008), 165–182.

[13] Levine D., A parallel genetic algorithm for the set partitioning problem. *PhD Thesis*, Illinois Institute of Technology / Argonne National Laboratory (1994)